Journal of
Composites Science

MDPI

Article

Microstructure and Hydrogen Storage Properties of Composites Derived from Oxidized Alloy Glass in the System of Zr-Pd-Pt

Masakuni Ozawa [1,*], Naoya Katsuragawa [2,†], Masatomo Hattori [1,‡] and Hidemi Kato [3]

[1] Institute of Materials and Systems for Sustainability, Nagoya University, Furo, Chikusa, Nagoya 464-8603, Aichi, Japan
[2] Department of Materials Design Engineering, Graduate School of Engineering, Nagoya University, Furo, Chikusa, Nagoya 464-8603, Aichi, Japan
[3] Institute for Materials Research, Tohoku University, Katahira, Aoba, Sendai 980-8577, Miyagi, Japan
* Correspondence: ozawa@imass.nagoya-u.ac.jp or ozawa.m@nagoya-u.jp
† Current address: Nippon Steel Co., Minato, Wakayama 640-8555, Wakayama, Japan.
‡ Current address: Department of Applied Chemistry, Aichi Institute of Technology, Yakusa, Toyota 470-0392, Aichi, Japan.

Abstract

A study on the hydrogen storage of composite materials derived from alloy glass in the system of Zr-Pd-Pt was conducted through the integration of multiple methodologies. The alloy following heat treatment in air at temperatures ranging from 280 °C to 800 °C showed a precipitated structure comprising metallic Pd-Pt particles and a ZrO_2 matrix. In the sample treated at 280 °C, the spillover phenomenon of absorbed hydrogen was suggested. The plateau region of the hydrogen pressure–concentration (PCT) isotherm showed the gradient profiles for the samples oxidized at 400 °C, 600 °C, and 800 °C. In the equilibrium absorption process, the $\Delta H°$ of approximately 38 kJ/mol was proposed, and the highest storage of hydrogen was H/Pd = 0.61 by the sample oxidized in air at 600 °C. The temperature programmed reduction (TPR) results exhibited rapid hydrogen release behavior at temperatures ranging from 50 °C to 65 °C. The findings offer novel insights into the microstructure, fabrication process, and overall hydrogen absorption/desorption properties of the composites prepared from a Zr-Pd-Pt alloy glass.

Keywords: hydrogen storage; alloy glass; Pd; Pt; ZrO_2; composites; spillover

Academic Editors: Ashwath Pazhani and Andre Batako

Received: 11 June 2025
Revised: 28 August 2025
Accepted: 2 September 2025
Published: 13 October 2025

Citation: Ozawa, M.; Katsuragawa, N.; Hattori, M.; Kato, H. Microstructure and Hydrogen Storage Properties of Composites Derived from Oxidized Alloy Glass in the System of Zr-Pd-Pt. *J. Compos. Sci.* **2025**, *9*, 563. https://doi.org/10.3390/jcs9100563

1. Introduction

A significant amount of research has been conducted on hydrogen storage under various conditions, including high-pressure hydrogen, liquid hydrogen, and solid-state hydrogen storage [1]. The development of novel materials that can absorb and store hydrogen has enabled more efficient utilization of this resource. These materials offer advantages such as low-pressure storage and high volumetric storage density, enabling reversible hydrogen absorption and desorption under moderate pressure and temperature conditions [2–5].

Metallic glassy materials represent the ultimate state of solid metastability, as evidenced by their benefits in a variety of potential application areas [6–8]. Additionally, due to the feasibility of preparing amorphous alloys through advanced processing techniques using large extended compositions, metallic glass can serve as a potential raw material [9,10]. The oxidation of metallic glass has revealed the synergistic effects of materials [11–14]. As an alternative proposition, composites in the metal–ceramic system are likely to generate

significant interest as a new class of hydrogen-related materials [15–18]. A notable example of prior studies is the investigation of nanocrystalline metal-ceramic composites consisting of Pd particles embedded in a ZrO_2 matrix, which are formed upon heat treatment in air [19–24]. Pd is a typical hydrogen storage metal, and Pd-based glass and the system of Pd and Zr have received attention regarding their hydrogen energy-related properties [25–28]. Researchers have demonstrated a keen interest in the hydrogen storage properties of Zr-Pd alloys following treatment in air, as evidenced by several reports [29,30], and preliminary findings on Pd/ZrO_2 composites have been documented [31–33]. However, the oxidized composite material derived from alloy glass in the system of Zr-Pd-Pt has not yet been examined in relation to its hydrogen storage potential.

The objective of this study is to investigate the preparation and hydrogen absorption and release properties of composites derived from oxidized alloy glass in the system of Zr-Pd-Pt. Platinum (Pt) lacks inherent hydrogen storage properties in its bulk state, and Pd and Pt are immiscible systems [34–36]. However, the nanoparticles (NPs) in the Pd-Pt system showed the hydrogen storage ability at low pressure [37–40]. The findings have prompted further investigation, which may offer significant advantages in terms of efficiency and performance. Conversely, the stabilization processing of the NPs in the composite is generally imperative, as very fine powder materials, when unsupported, are less efficient for handling and H_2 storage/release operations. The processing of Pd-Pt nanoparticle materials is also not straightforward; for example, seed-controlled core–shell-type Pt-Pd NPs must be designed using multi-step solution methods [36,37]. In addition, the particles must be followed by a final immobilization process in a matrix solid. Therefore, it is necessary to develop innovative and simple methods for the preparation of these composites. Alloy glass-driven composites, containing metal particles, will be a candidate for easily processed hydrogen storage materials in multicomponent systems.

In this study, the microstructural development of composites is examined as a derivative of alloy glass to form the composite. Subsequently, hydrogen isotherm measurements are conducted to investigate the interaction and reactivity of hydrogen gas over the resulting composites. The correlation between the precipitated structure, particularly metallic Pd-Pt particles, and PCT results was examined with the proposed model concerning hydrogen interaction. Furthermore, the H_2 dynamic release properties of the composite were examined in the heat cycle after H_2 absorption. The present study proposes a novel approach to form composites with hydrogen storage capabilities by utilizing a metallic glass as a starting material in the system of Zr-Pd-Pt.

2. Experimental Methods

2.1. Sample Preparation

The initial alloy glass was prepared according to the following procedure. The mixture of 99.6 wt% pure zirconium, 99.99 wt% pure palladium, and 99.99 wt% pure platinum metal was melted in a purified argon (Ar) atmosphere on a water-cooled copper mold in an arc furnace [41]. The chemical composition of the alloy was determined to be $Zr_{65}Pd_{30}Pt_5$, which corresponds to the atomic ratio. Samples of the ribbon form with a thickness of approximately 0.02 mm and a width of approximately 1 mm were prepared from the molten alloy using the single-roll melt-quench spinning method in an Ar atmosphere. The resulting alloy glass was subsequently heated in air at 280 °C for 24 h and 400 °C, 600 °C, and 800 °C for 3 h.

2.2. Characterization

The crystal phases of the specimen were analyzed with an XRD apparatus (Rigaku MiniFlex, Tokyo, Japan) with Cu Kα radiation at 15 kV and 30 mA. The data were collected

at a scanning rate of 1°/min with a step size of 0.02° in the 2θ range between 20 and 80°. The crystallite size of the metal phase (Pd-Pt) was calculated with the Scherrer equation using a peak of 2θ = 40°. A field emission scanning electron microscopy device (FE-SEM; Hitachi S-4800, Tokyo, Japan) at 15 keV was used for the observation of the microstructures of the samples. The chemical element mapping images were also obtained for the selected samples using an energy-dispersive spectroscopy (EDS) device equipped in the SEM.

2.3. Evaluation of Hydrogen Storage

The evaluation of hydrogen storage properties was conducted with a gas volumetric apparatus (Microtruck Bell Belsorp-max, Tokyo, Japan). First, 0.5 g of the sample was loaded into the chamber. The hydrogen pressure–concentration isotherm (denoted as PCT) was obtained at different temperatures of 30 °C, 45 °C, and 60 °C. The initial measurement at 60 °C was used as a pretreatment, and then the measurements were obtained at 30 °C, 45 °C, and 60 °C in that sequence. The dead volume of the sample chamber was measured at each temperature, and the samples were vacuum-evacuated to remove absorbents. This procedure was repeated for the subsequent measurements at the next temperature. During the PCT measurements, the samples were held at each pressure for 60 s to reach an equilibrium state before moving to the next pressure. The temperature-dependent PCT data were analyzed using the van't Hoff equation to derive the thermodynamic constants.

2.4. Evaluation of Dynamic Hydrogen Absorption/Release

The dynamic behaviors of H_2 absorption and release were observed with a temperature-programmed reduction (TPR) apparatus (BP-1S, Henmi Slide-rule Co., Ltd., Tokyo, Japan) equipped with an online thermal conductivity gas detector (TCD). In the absorption experiment, the sample was heated to 150 °C for 20 min, followed by cooling to 30 °C in flowing Ar. Subsequently, the Ar gas was switched to 5% H_2/Ar mixture flow at 30 °C, where it was maintained for 20 min for the next H_2 release experiment. In the H_2 release experiment, the subsequent desorption experiment was followed by gradual heating at a rate of 10 °C min^{-1} from 30 °C to 150 °C. The occurrence of hydrogen release from the sample was indicated by the observation of a peak signal in the reverse direction. The signal of TCD corresponds to the differential of H_2 concentration with respect to time, allowing for the observation of the absorbing and releasing behavior (rate change).

3. Results and Discussion

3.1. Crystal Phase and Microstructure of Composites

Figure 1 shows a series of XRD patterns of the $Zr_{65}Pd_{30}P_{t5}$ after heat treatment in air at 280 °C for 24 h and 400, 600, and 800 °C for 3 h. The XRD patterns of the samples showed phase and structural transformations from the amorphous state to the mixture of crystalline phases by heat treatment. The samples contained metallic Pd, PdO, and ZrO_2, consisting of a mixture of tetragonal (t) and monoclinic (m) phases. Regarding Pd composition, the predominant crystallized phase was PdO (2θ = 34°), and the formation of metallic Pd was also observed via a weak diffraction peak at around 2θ = 40°. The fraction of the metallic Pd phase increased with heat treatment at 800 °C. The absence of a distinct Pt phase was attributed to the limitations in crystallinity of the Pd phase and the solute contribution of Pt.

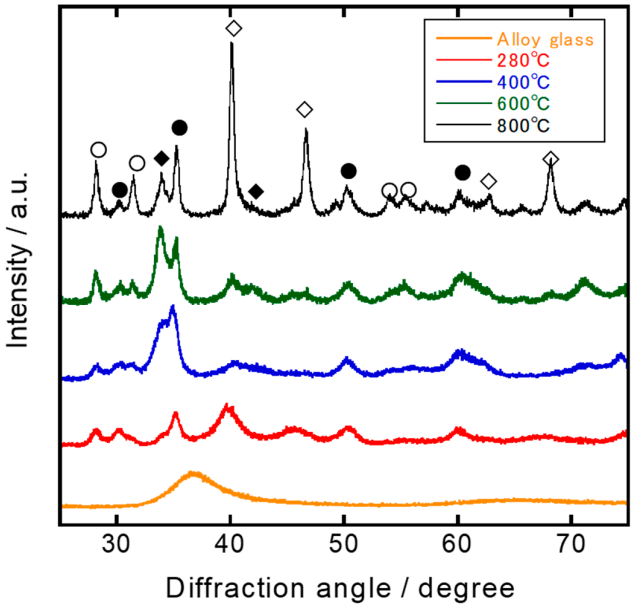

Figure 1. The XRD patterns of the initial and oxidized $Zr_{65}Pd_{30}Pt_5$ alloy glasses after heat treatment in air at 280 °C for 24 h and 400 °C, 600 °C, and 800 °C for 3 h, respectively. ♢: Pd, ♦: PdO, ○: m-ZrO_2, ●: t-ZrO_2.

Figure 2 shows the SEM images of the morphology of the $Zr_{65}Pd_{30}P_{t5}$ after heat treatment in air at 280 °C for 24 h and 400 °C, 600 °C, and 800 °C for 3 h, respectively. The microstructure indicated the formation of the composite in which granular precipitates were dispersed in the matrix. Precipitates with diameters ranging from approximately 10 nm to 2 μm appeared on the surface. The average grain size of the particles was 36 nm (280 °C), 92 nm (400 °C), 210 nm (600 °C), and 408 nm (800 °C), respectively, where the values in parentheses represent the heat treatment temperatures (HTTs).

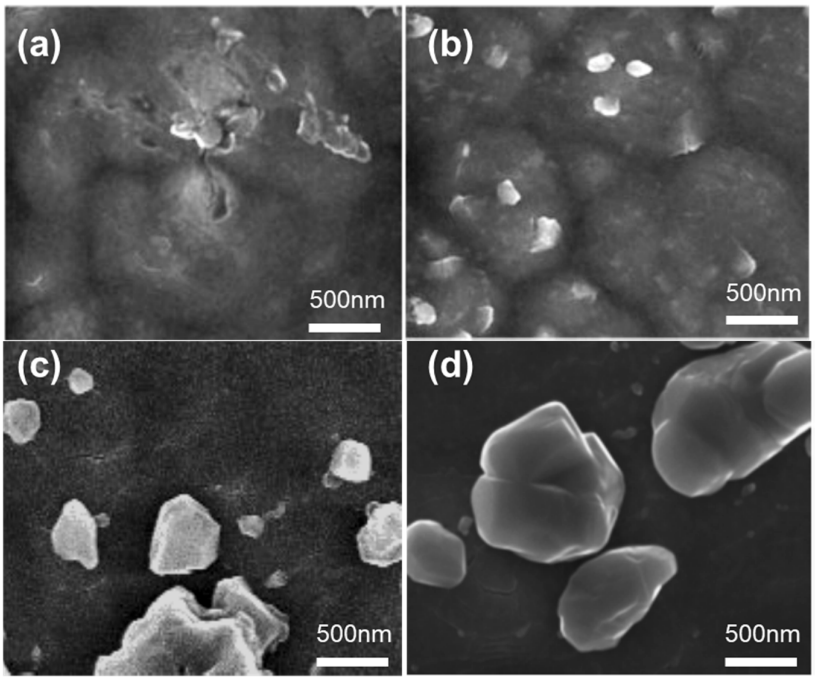

Figure 2. The SEM images of the oxidized $Zr_{65}Pd_{30}Pt_5$ alloy glasses after heat treatment in air at 280 °C for 24 h (**a**) and 400°C (**b**), 600°C (**c**), and 800 °C (**d**) for 3 h, respectively.

Figure 3 shows the sets of the SEM and the chemical elemental mapping image of the sample heated in air at 600 °C for 3 h, revealing the presence of the precipitates. The elemental distribution indicates that these precipitates mainly consist of Pd and are embedded in the ZrO_2 matrix. Although the image of the distribution of Pt exhibited low contrast in the figures, its existence appeared to be analogous to that of Pd. The Pd (Pt) phase in these composites was broadly characterized as being isolated in the matrix ZrO_2.

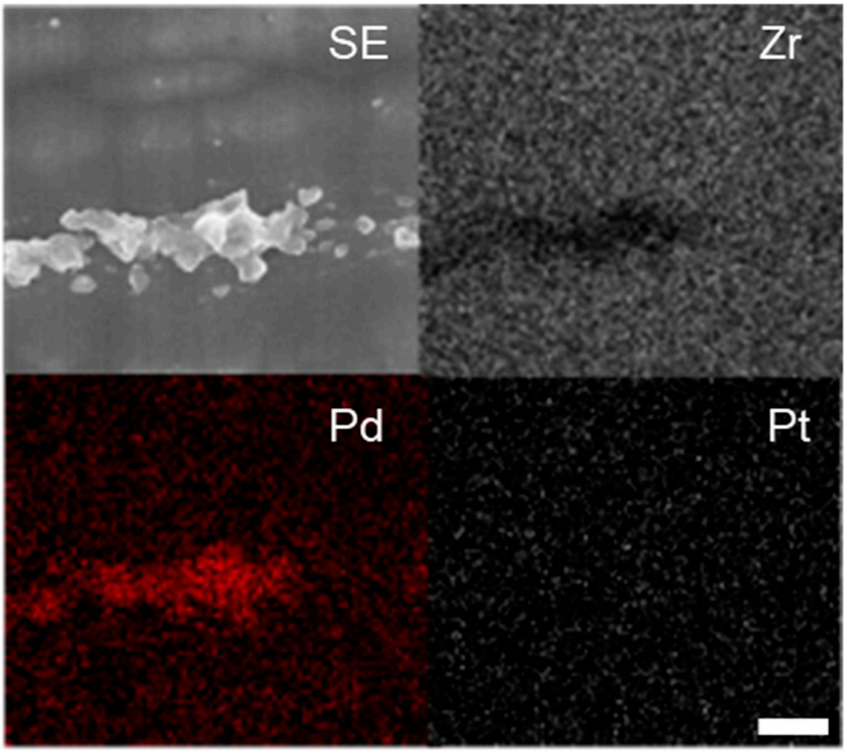

Figure 3. The SEM and EDS element (Zr, Pd, and Pt) mapping images of a precipitate in the oxidized $Zr_{65}Pd_{30}Pt_5$ at 600 °C for 3 h.

Figure 4 shows the XRD patterns of the samples, which were obtained after PCT measurement. They demonstrate that the PdO phase underwent a transformation into metallic Pd following mild H_2 treatment across all samples. However, no discernible morphological alterations were observed in the samples after PCT measurement. As illustrated in Figure 4b, the XRD peaks of Pd (111) exhibited broad features. The d-spacing of Pd-Pt (111), assuming the presence of a single peak, was calculated to be 0.225_8 nm (280 °C), 0.225_0 nm (400 °C), 0.224_9 nm (600 °C), and 0.225_0 nm (800 °C), where the values in parentheses represent HTT. The fraction of Pd was calculated using the d-spacing of Pd (111) (0.2246 nm) and Pt (111) (0.2265 nm). The resulting values for x were 0.36 (280 °C), 0.84 (400 °C), 0.81 (600 °C), and 0.84 (800 °C), respectively, for Pd_xPt_{1-x}. The values were consistent with the starting composition of Pd and Pt, i.e., x = 0.857, within the error range under conditions where HTT exceeded 400 °C. In the case of 280 °C, the Pt metal phase appears to precipitate initially, forming Pt-rich crystallites. The crystallite size of the Pd phase particles was found to be 5.3 nm (280 °C), 7.8 nm (400 °C), 11.0 nm (600 °C), and 26.0 nm (800 °C), respectively. It was observed that both crystallite and grain sizes increased with increasing HTT. The former was smaller than the latter, indicating the precipitates of the polycrystalline grains.

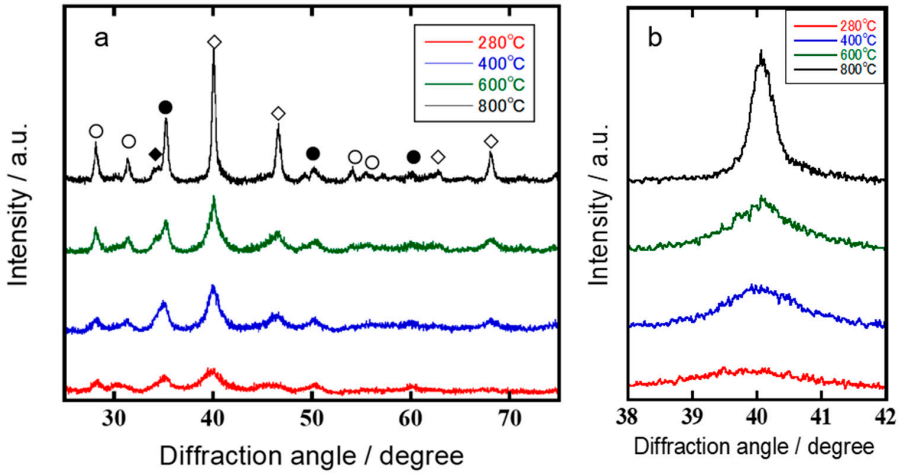

Figure 4. The XRD patterns of the oxidized $Zr_{65}Pd_{30}Pt_5$ alloy glasses after heat treatment in air at 280 °C for 24 h and 400 °C, 600 °C, and 800 °C for 3 h, respectively, followed by PCT measurement. ◇: Pd; ◆: PdO; ○: m-ZrO_2; •: t-ZrO_2. (**a**) Full chart, (**b**) Selected chart.

3.2. PCT Isotherms

Figure 5 shows the PCT isotherms versus the hydrogen-to-platinum (H/Pd) ratio at 30 °C for four samples, which were prepared at 280, 400, 600, and 800 °C, respectively. These isotherms reveal the distinct behavior exhibited by the samples in terms of hydrogen absorption. Notably, pure Pd generally exhibits a pressure plateau in relation to the H/Pd atomic ratio [4,5]. However, the line corresponding to the sample oxidized at 280 °C showed a monotonic increase in hydrogen amount versus pressure on the logarithmic scale. Conversely, the samples prepared at 400 and 600 °C exhibited a plateau region within gradient isotherms. In contrast, the samples oxidized at 800 °C also showed the gradient isotherm, though the plateau region was comparatively diminished in terms of hydrogen storage capacity. The hydrogen storage capacity from the plateau region evaluated in the present experiment was determined to be H/Pd = 0.30, 0.61, and 0.20 for the sample oxidized at 400 °C, 600 °C, and 800 °C, respectively.

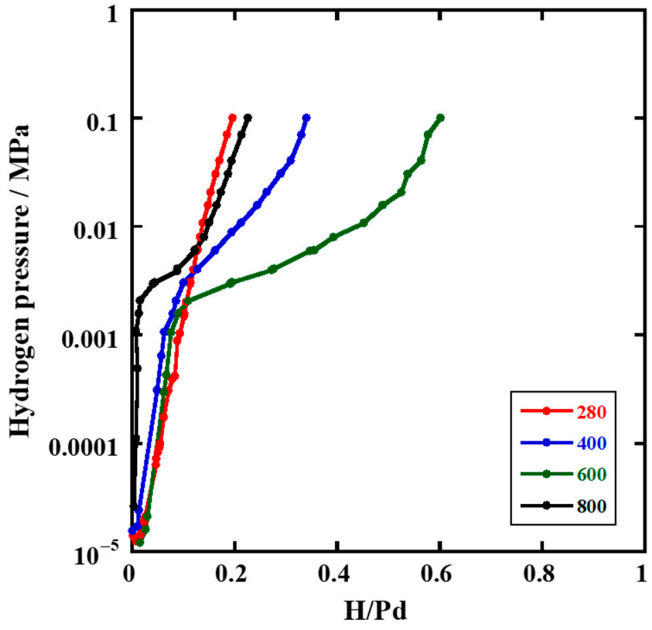

Figure 5. Hydrogen absorption isotherms at 30 °C of the oxidized $Zr_{65}Pd_{30}Pt_5$ alloy glasses after heat treatment in air at 280 °C for 24 h (red) and 400 °C (blue), 600 °C (green), and 800 °C (black) for 3 h, respectively.

Figure 6a–d show the temperature-dependent hydrogen storage behaviors of the four samples, representing the PCT curves at 30 °C, 45 °C, and 60 °C, respectively. As the temperature increased, the curves shifted to higher pressure. As shown in Figures 5 and 6, a novel observation has been made concerning the difference between the oxidized $Zr_{65}Pd_{30}Pt_5$ sample at different temperatures. It is assumed that this phenomenon is influenced by both the matrix and the intrinsic effects on the Pd-based metal phase in these composites. The amount of absorbed hydrogen appears to be contingent on the pressure; however, the profile in the oxidized sample at 280 °C (Figure 6a) seems to represent a monotonic relation between log P_{H2} vs. H/Pd. In contrast, the samples oxidized at 400 °C and 600 °C (Figure 6b,c) show hydrogen absorption behavior, characterized by a plateau region with a gradient. Initially, the amount of hydrogen absorbed increased logarithmically with hydrogen pressure before reaching the plateau region. The samples oxidized at 800 °C (Figure 6d) exhibited an analogous hydrogen absorption behavior, although the maximum H/Pd appeared to be reduced.

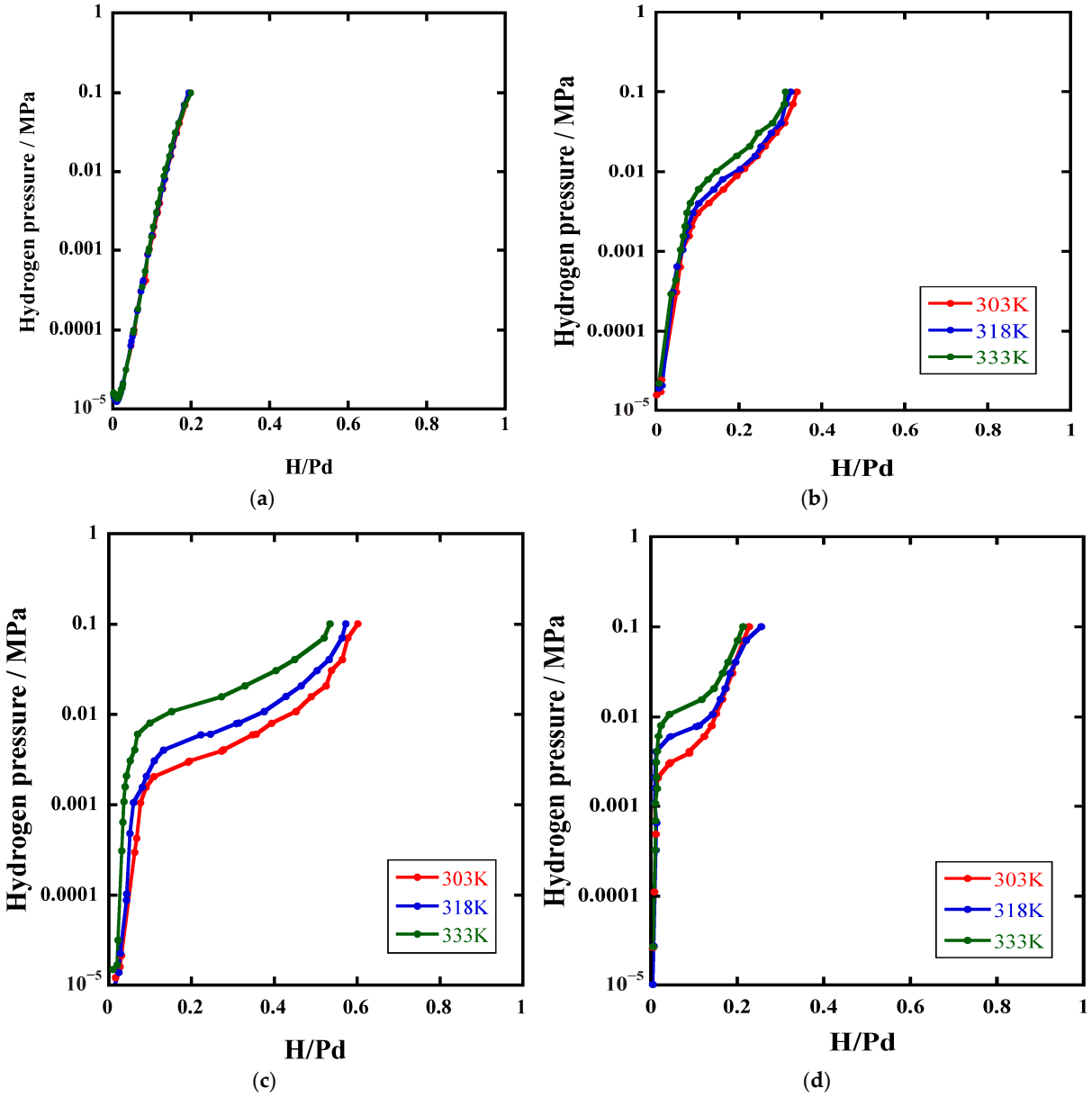

Figure 6. Hydrogen absorption isotherms of the oxidized $Zr_{65}Pd_{35}$ samples after heat treatment in air at 280 °C for 24 h (**a**) and 400 °C (**b**), 600 °C (**c**), and 800 °C (**d**) for 3 h, measured at 30 °C (red), 45 °C (blue), and 60 °C (green), respectively.

The isotherm of the oxidized sample at 280 °C lacks a plateau region, showing a different isotherm profile from that of the other three samples. Solid hydrogenation is generally initiated by the presence of dissociated hydrogen, which directly interacts with the solid surfaces. The remarkable absorption of ZrO_2 itself has not been previously documented. The solubility of hydrogen in ZrO_2 at temperatures between 500 and 1000 °C was measured to decrease with increasing hydration temperature from $\sim 10^{-4}$ to $\sim 10^{-5}$ H per ZrO_2 [42]. The catalytic hydrogenation mechanism involves hydrogen activation on a dispersed metallic surface, often followed by the atomic hydrogen spillover behavior on supports. The phenomenon of hydrogen spillover is defined as the transport of activated hydrogen across a solid surface/interface, and a number of sites should be replaced by the spillover sites near metal atoms and/or clusters (interface besides the ZrO_2 matrix). This occurs as a hydrogen flow via the Pd surface to the interface before the formation of the metal hydride.

The gas adsorption of porous media is represented by the Dubinin–Radushkevich (D–R) Equation (1) [43,44], as follows:

$$a = a_0 \exp (A/E)^2 \quad (1)$$

where a is the value of adsorption, and a_0 is the limiting value, which is a function of micropore volume. $A = -RTln(P/P_0)$ is the differential molar work of adsorption; P is pressure and P_0 is the standard pressure (usually the saturation pressure); R is the gas constant; T is the absolute temperature; and E is the characteristic energy of adsorption, which is a function of the pore radius. The function establishes a linear relationship between ln(a) and the function $f = -RTln(P/P_0)^2$. This has been observed and applied to the hydrogen storage of carbonaceous materials and MOF complexes [45]. Figure 7 shows the plot of a profile of the oxidized sample at 280 °C and indicates a well-fitted result in the wide range of H/Pd. The SEM images of the present composite (Figure 2a) show the uneven surface of the ZrO_2 matrix with fine, irregularly shaped precipitates. In consideration of the chemical process involved in the spillover of hydrogen on the metal/support system, it is postulated that the composite may undergo continuous absorption of hydrogen within its porous surface. A portion of the palladium does not coalesce into a substantial metal domain but rather into smaller clusters. These are incapable of readily storing hydrogen within metal lattices but instead send it into the interface and/or pore surfaces.

A series of profiles from three other composites oxidized at 400 °C, 600 °C, and 800 °C, respectively, showed the plateau regions with a gradient. These plateau regions appear to be indicative of a balance between two hydrogen pick-up stages. Consequently, a transition from spillover-type hydrogen to hydrogen storage within Pd-based metal particles, surrounded by a ZrO_2 matrix, is anticipated. However, the fraction of these particles varies depending on the crystallite size, which is influenced by the different HTT.

In recent research, Pd NPs have emerged as a new class of hydrogen storage materials [46–49]. Bardhan et al. examined hydrogen storage in metal hydride systems, particularly focusing on an intrinsic size-scaling law for hydriding transformations in manomaterials [47]. For example, the fraction of one layer unit (a = 0.39 nm) of the surface was estimated to affect final hydrogen storage in Pd, and the ratio of H/Pd was determined to be 0.48 for Pd NP with 4 nm in diameter. The PdHx phase must undergo growth within a strained crystal lattice in each nanoparticle. The hydrogen storage capacity is diminished by very small clusters and/or nanocrystals, in the isolated state, due to the presence of non-bulky crystal lattices. Also, the polycrystalline crystallites in the grains of 20–70 nm were understood to exhibit similar characteristics to isolated nanocrystals during a hydride phase transformation [50].

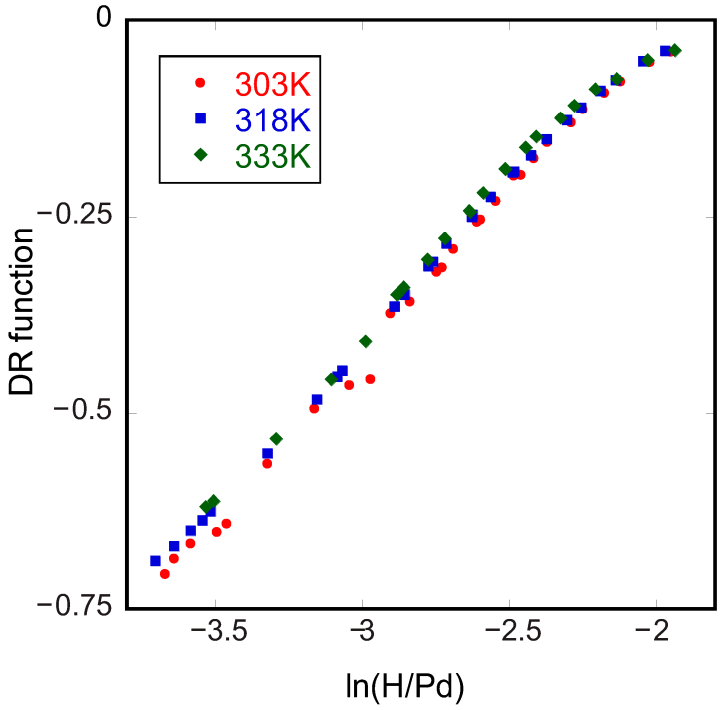

Figure 7. Dubinin–Radushkevich (D–R) plots of ln(H/Pd) versus DR function (= $-RT\ln(P/P_0)^2$) for the oxidized $Zr_{65}Pd_{30}Pt_5$ samples after heat treatment in air at 280 °C.

In addition, since Pt alone does not form a hydride, the subunit of Pt in the alloyed crystal unit of Pd-Pt cannot stabilize hydrogen in the bulk lattice as a hydride [36]. However, a hydrogen storage phenomenon has been reported for core–shell structured Pd-Pt NPs by focusing on the interfacial properties [39]. For the Pd-Pt alloy composite, hydrogen storage can be observed, even when the pressure is far lower than the equilibrium condition of hydride formation.

It is noteworthy that the present H/Pd of a sample oxidized at 600 °C was found to be a large capacity of H/Pd = 0.61, which is comparable to that of a Pd black powder [49]. The crystallite size of the Pd-Pt particle in the present sample was approximately 10 nm. The specific surface area from the measurement of nitrogen adsorption at 77K was 20 m^2g^{-1}. It is suggested that the relatively substantial hydrogen storage capacity is attributable to the application of nanoparticulate Pd-Pt and the embedding of NPs within a matrix in a composite. This phenomenon can be ascribed to the strain relaxation at the interface between metal NPs and a matrix. While the maximum H/Pd of the samples oxidized at 800 °C is reduced, this is due to the inhibition of the hydride phase in the Pd-Pt solid solution following grain growth. The generation of the current PCT isotherms is influenced by a multitude of factors, including the state of the NPs, the Pd-Pt alloy, and the impact of the matrix effects. Consequently, the optimization of the nanostructure for hydrogen storage capacity is achieved by selecting the heat treatment temperature for a starting alloy glass.

Finally, the thermodynamics of hydrogen storage are discussed. For a reaction (2) between a metal M and hydrogen, the thermodynamics are described by the van't Hoff relation (3) [51,52]:

$$M + (x/2)H_2 \rightarrow MH_x \quad (2)$$

$$\ln p_{H_2} = \frac{\Delta H^o}{RT} - \frac{\Delta S^o}{R} \quad (3)$$

where ΔH° and ΔS° are the equilibrium enthalpy and entropy changes, respectively, and R is the gas constant. The equilibrium pressure of hydrogen, pH_2, in the plateau region is

related to the absolute temperature T. The plateau pressures increased due to the decreased stability of the hydride phase. The PCT curves of three samples (oxidized at 400 °C, 600 °C, and 800 °C) exhibited such a shift with respect to the plateau pressure, depending on the measurement temperature.

The van't Hoff plots from the PCT profiles for three samples prepared at each HTT are shown in Figure 8. Table 1 shows the measured ΔH° and ΔS° of the three samples. For the samples (HTT), ΔH° was -38.0 ± 5.1 kJ/mol (for 400 °C), -37.8 ± 3.2 kJ/mol (for 600 °C), and -37.9 ± 2.0 kJ/mol (for 800 °C). The calculated ΔH° for the hydride phase formation in these samples was approximately -38 kJ/mol. While the ΔH° was slightly larger than that of pure Pd, the bulk properties remain constant for the hydride formation reaction in the composites. Table 2 presents a comparison of the experimental ΔH° values for the absorption of hydrogen in Pd-Pt alloy particles [37,52,53]. The present ΔH° was found to be less substantial in comparison with the other data pertaining to isolated Pd-Pt particles. This phenomenon is likely attributable to the microstructure of the composite, which is composed of nanoparticle-embedded ZrO_2. Upon the entry of the hydrogen atom into the nanoparticle to form a hydride domain, a strain is induced between the surface and the inner part of a metal hydride particle. This phenomenon can be understood as an increase in the enthalpy of the nanoparticle state, accompanied by a corresponding rise in its instability. Conversely, the strain will be relaxed by the consistent adhesion between the embedded Pd-Pt particles and a ZrO_2 matrix at the interface. The present value of ΔH° indicates a tendency for the stabilization of the hydride phase in comparison with the isolated nanoparticle state. It is also noteworthy that the mixing phase of Pd and Pt exhibits the H_2 storage properties at low hydrogen pressures (10^{-3}–10^{-4} MPa in Figure 5) when the metal phase was dispersed in the ZrO_2 matrix.

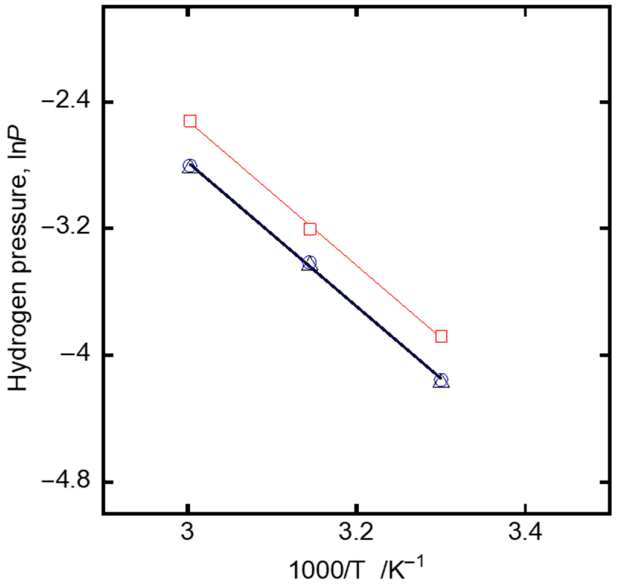

Figure 8. Van't Hoff plots of the oxidized $Zr_{65}Pd_{30}Pt_5$ samples after heat treatment in air at 400 °C (blue), 600 °C (purple green), and 800 °C (red) for 3 h.

Table 1. ΔH° and ΔS° of the samples. Due to the absence of a plateau in the data at 280 °C, the parameters could not be obtained.

Sample (HTT)	280 °C	400 °C	600 °C	800 °C
ΔH/kJ mol^{-1}	-	−38.1	−37.8	−37.9
ΔS/J mol^{-1}	-	−91.5	−91.5	−92.9

Table 2. Comparison of ΔH° for the Pd-Pt nanoparticles.

Composition	Diameter	ΔH°/kJ mol^{-1}	Ref.
$Pd_{0.86}Pt_{0.14}$	5–26 nm	−37.8–−38(±5)	This study
$Pd_{0.95}Pt_{0.05}$	74 μm	−29.1	[53]
$Pd_{0.92}Pt_{0.08}$	6.7 nm	−30	[37]
$Pd_{0.85}Pt_{0.15}$	7.4 nm	−24.5	[37]
$Pd_{0.80}Pt_{0.20}$	5.1 nm	−20.7	[54]

3.3. H_2 Absorption/Desorption Behavior

Figure 9a shows a series of TPR profiles for the H_2 absorption behaviors at 30 °C. In this figure, the time-dependent change in the gaseous H_2 concentration is observed when switching the Ar gas to the 5% H_2/Ar mixture flow. Since the first run was unstable, the profiles are shown in the second run. The absorption of hydrogen in the downward direction is found after the introduction of H_2 at 135 s. They show that the spontaneous absorbing behavior of H_2 in the solid can be achieved on the present composites with the multi-step process, except for a sample oxidized at 280 °C. The delayed and complex signals with time lag suggest a diffusion-limited H_2 absorption phenomenon of distributed-sized metal precipitates in the ribbon sample.

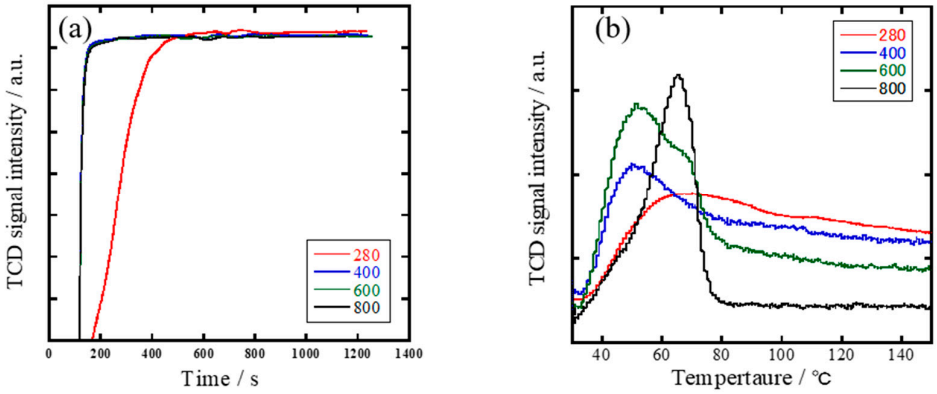

Figure 9. The TPR profile of absorption and release of H_2. Panel (**a**): The H_2-TPR profile of the four Pd/ZrO_2 samples. The heat treatment condition is in air at 280 °C for 24 h (red and 400 °C (blue), 600 °C (green), and 800 °C (black) for 3 h, respectively, as a reference to Pd black (black). Panel (**b**): The TPR profile of hydrogen release during the heating ramp experiment. The samples are the same as in (**a**).

Figure 9b shows the H_2 release properties of the composites during the heat-up stage in the second TRR runs. The profile of a sample oxidized at 280 °C exhibited a very broad signal, suggesting difficulty in rapidly recovering spillover hydrogen. In the remaining three samples, the gas phase concentration rate of H_2 exhibited an increase at temperatures ranging from 50 °C to 65 °C (the inset in Figure 9a) during a heating ramp. It is noteworthy that the release peaks of H_2 in the samples were observed to be lower than the same evaluation that yielded a peak of Pd black powder at 79 °C. The main release peak was observed at 50 °C for the composite oxidized at 600 °C. Therefore, the Pd-Pt/ZrO_2 composite has been found to have advantages in terms of the rapid operation of H_2 recovery at lower temperatures.

4. Conclusions

In this study, the formation and hydrogen storage of composite materials derived from alloy glass in the system of Zr-Pd-Pt are discussed. The results yielded the novel properties

of the overall hydrogen absorption/desorption, indicating a new type of hydrogen storage material. The findings were as follows:

1. The XRD and surface morphology of the alloy glass after heat treatment in air at 280–800 °C showed a precipitated structure consisting of metallic Pd-Pt particles on the matrix of ZrO_2.
2. The PCT isotherms of the composites exhibited the characteristic hydrogen absorption behaviors. In the equilibrium absorption process, the amount of the stored H_2 reaches its maximum of H/Pd = 0.61 in the composite prepared at 600 °C. The ΔH° of approximately 38 kJ/mol was for the hydride formation reaction.
3. The H_2-TPR results demonstrated the hydrogen absorption/release behavior on the composite. The desorption of H_2 occurred at relatively low temperatures ranging from 50 °C to 65 °C at atmospheric pressure.

Author Contributions: M.O.: conceptualization, methodology, investigation, writing—original draft, writing—review and editing, supervision, project administration, and funding acquisition. N.K.: validation, data curation, and investigation. M.H.: methodology, validation, data curation, and investigation. H.K.: investigation, supervision, project administration, and funding acquisition. All authors have read and agreed to the published version of the manuscript.

Funding: This work was supported by the Projects of the Design and Engineering by Joint Inverse Innovation for Materials Architecture (DEJI^{2}MA) and the Life Innovation Materials for Interdisciplinary and International Researcher Development of the Ministry of Education, Culture, Sports, Science and Technology, Japan.

Data Availability Statement: The original contributions presented in this study are included in the article. Further inquiries can be directed to the corresponding author.

Acknowledgments: The authors are grateful to K. Kobayashi and S. Yamaura for their help with the machine control and sample processing.

Conflicts of Interest: The authors declare no conflict of interest.

References

1. Moradi, R.; Groth, K.M. Hydrogen Storage and Delivery: Review of the State of the Art Technologies and Risk and Reliability Analysis. *Int. J. Hydrogen Energy* **2019**, *44*, 12254–12269. [CrossRef]
2. Niaz, S.; Manzoor, T.; Pandith, A.H. Hydrogen Storage: Materials, Methods and Perspectives. *Renew. Sustain. Energy Rev.* **2015**, *50*, 457–469. [CrossRef]
3. Nivedhitha, K.S.; Beena, T.; Banapurmath, N.R.; Umarfarooq, M.A.; Ramasamy, V.; Soudagar, M.E.M.; Ağbulut, Ü. Advances in Hydrogen Storage with Metal Hydrides: Mechanisms, Materials, and Challenges. *Int. J. Hydrogen Energy* **2024**, *61*, 1259–1273. [CrossRef]
4. Singh, G.; Ramadass, K.; DasiReddy, V.D.B.C.; Yuan, X.; Sik Ok, Y.; Bolan, N.; Xiao, X.; Ma, T.; Karakoti, A.; Yi, J.; et al. Material-Based Generation, Storage, and Utilisation of Hydrogen. *Prog. Mater. Sci.* **2023**, *135*, 101104. [CrossRef]
5. Klopčič, N.; Grimmer, I.; Winkler, F.; Sartory, M.; Trattner, A. A review on metal hydride materials for hydrogen storage. *J. Energy Storage* **2023**, *72*, 108456. [CrossRef]
6. Löffler, J.F. Bulk Metallic Glasses. *Intermetallics* **2003**, *11*, 529–540. [CrossRef]
7. Inoue, A.; Takeuchi, A. Recent Development and Application Products of Bulk Glassy Alloys. *Acta Mater.* **2011**, *59*, 2243–2267. [CrossRef]
8. Jiang, R.; Da, Y.; Chen, Z.; Cui, X.; Han, X.; Ke, H.; Liu, Y.; Chen, Y.; Deng, Y.; Hu, W. Progress and Perspective of Metallic Glasses for Energy Conversion and Storage. *Adv. Energy Mater.* **2022**, *12*, 2101092. [CrossRef]
9. Schroers, J. Processing of Bulk Metallic Glass. *Adv. Mater.* **2010**, *22*, 1566–1597. [CrossRef]
10. Halim, Q.; Mohamed, N.A.N.; Rejab, M.R.M.; Naim, W.N.W.A.; Ma, Q. Metallic Glass Properties, Processing Method and Development Perspective: A Review. *Int. J. Adv. Manuf. Technol.* **2021**, *112*, 1231–1258. [CrossRef]
11. Zhang, M.; Huang, T.; Zhang, J.; Deng, L.; Gong, P.; Wang, X. Influence of Oxidation on Structure, Performance, and Application of Metallic Glasses. *Adv. Mater.* **2022**, *34*, 2110365. [CrossRef]

12. Zhou, W.H.; Duan, F.H.; Meng, Y.H.; Zheng, C.C.; Chen, H.M.; Huang, A.G.; Wang, Y.X.; Li, Y. Effect of Alloying Oxygen on the Microstructure and Mechanical Properties of Zr-Based Bulk Metallic Glass. *Acta Mater.* **2021**, *220*, 117345. [CrossRef]
13. Li, F.; Zhang, Z.; Liu, H.; Zhu, W.; Wang, T.; Park, M.; Zhang, J.; Bönninghoff, N.; Feng, X.; Zhang, H.; et al. Oxidation-Induced Superelasticity in Metallic Glass Nanotubes. *Nat. Mater.* **2024**, *23*, 52–57. [CrossRef] [PubMed]
14. Köster, U.; Jastrow, L. Oxidation of Zr-Based Metallic Glasses and Nanocrystalline Alloys. *Mater. Sci. Eng. A* **2007**, *449–451*, 57–62. [CrossRef]
15. Pentimalli, M.; Imperi, E.; Bellusci, M.; Alvani, C.; Santini, A.; Padella, F. Silica-Metal Composite for Hydrogen Storage Applications. *Crystals* **2012**, *2*, 690–703. [CrossRef]
16. Srinivasan, S.; Demirocak, D.E.; Kaushik, A.; Sharma, M.; Chaudhary, G.R.; Hickman, N.; Stefanakos, E. Reversible Hydrogen Storage Using Nanocomposites. *Appl. Sci.* **2020**, *10*, 4618. [CrossRef]
17. Nagar, R.; Srivastava, S.; Hudson, S.L.; Amaya, S.L.; Tanna, A.; Sharma, M.; Achayalingam, R.; Sonkaria, S.; Khare, V.; Srinivasan, S.S. Recent Developments in State-of-the-Art Hydrogen Energy Technologies—Review of Hydrogen Storage Materials. *Sol. Compass* **2023**, *5*, 100033. [CrossRef]
18. Rahman, M.A.; Taher, A.; Mia, R.; Chowdhury, F.I.; Khandaker, M.U.; Osman, H.; Hossain, M.K.; Al-Sehemi, A.G.; Ghann, W.; Alim, M.A.; et al. Deciphering the Mechanisms and Contributions of Ceramic-Based Materials in Hydrogen Storage Applications: A Contemporary Outlook. *Chem. Pap.* **2024**, *78*, 7685–7705. [CrossRef]
19. Müller, C.A.; Maciejewski, M.; Koeppel, R.A.; Baiker, A. Combustion of Methane over Palladium/Zirconia Derived from a Glassy Pd–Zr Alloy: Effect of Pd Particle Size on Catalytic Behavior. *J. Catal.* **1997**, *166*, 36–43. [CrossRef]
20. Kimura, H.; Inoue, A.; Masumoto, T. Production of nanocrystalline ZrO_2 and Pd composites by oxidation of an amorphous $Zr_{65}Pd_{35}$ alloy. *Mater. Lett.* **1992**, *14*, 232–236. [CrossRef]
21. Ozawa, M.; Masuda, A.; Nakamura, M.; Hattori, M.; Kato, H.; Yamamura, S. Soot-Combustion Catalyst of Pd/ZrO_2 Composites Prepared from $Zr_{65}Pd_{35}$ Amorphous Alloy by Oxidation Treatment. *Jpn. J. Appl. Phys.* **2020**, *59*, SAAC06. [CrossRef]
22. Hattori, M.; Ozawa, M.; Masuda, A.; Yamaura, S. Microstructure, surface properties, and CO oxidation properties of oxidized Zr_2Pd alloy glass. *Intermetallics* **2022**, *144*, 107510. [CrossRef]
23. Hattori, M.; Katsuragawa, N.; Yamaura, S.; Ozawa, M. Three-Way Catalytic Properties and Microstructures of Metallic Glass Driven Composite Catalysts. *Catal. Today* **2021**, *375*, 273–281. [CrossRef]
24. Kamiuchi, N.; Haneda, M.; Ozawa, M. Propene oxidation over palladium catalysts supported on zirconium rich ceria–zirconia. *Catal. Today* **2015**, *241*, 100–106. [CrossRef]
25. Sarac, B.; Sarac, A.S.; Eckert, J. Pd-based Metallic Glasses as Promising Materials for Hydrogen Energy Applications. *J. Electrochem. Soc.* **2023**, *170*, 014503. [CrossRef]
26. Somenkov, V.A.; Agafonov, S.S.; Glazkov, V.P.; Syrykh, G.F.; Verbetsky, V.N.; Yaropolov, Y.L. Hydrogen induced phase transitions in amorphous alloys. *Int. J. Hydrogen Energy* **2011**, *36*, 1209–1211. [CrossRef]
27. Berger, F.; Varga, M.; Mulas, G.; Molnár, Á.; Dékány, I. Surface Characteristics, Hydrogen Sorption, and Catalytic Properties of Pd−Zr Alloys. *Langmuir* **2003**, *19*, 3692–3697. [CrossRef]
28. Harris, J.H.; Curtin, W.A.; Tenhover, M.A. Universal Features of Hydrogen Absorption in Amorphous Transition-Metal Alloys. *Phys. Rev. B* **1987**, *36*, 5784–5797. [CrossRef]
29. Ning, J.; Zhang, X.; Qin, J.; Wang, L.; Passerone, D.; Ma, M.; Liu, R. Origin of Distinct Hydrogen Absorption Behavior of Zr_2Pd and $ZrPd_2$. *Int. J. Hydrogen Energy* **2016**, *41*, 1736–1743. [CrossRef]
30. Babai, D.; Bereznitsky, M.; Shneck, R.Z.; Jacob, I. The effect of Pd on hydride formation in $Zr(Pd_xM_{1-x})_2$ intermetallics where M is a 3d element. *J. Alloys Compd.* **2021**, *889*, 161503. [CrossRef]
31. Yamaura, S.-I.; Sasamori, K.-I.; Kimura, H.; Inoue, A.; Zhang, Y.C.; Arata, Y. Hydrogen Absorption of Nanoscale Pd Particles Embedded in ZrO_2 Matrix Prepared from Zr–Pd Amorphous Alloys. *J. Mater. Res.* **2002**, *17*, 1329–1334. [CrossRef]
32. Ozawa, M.; Kato, S.; Kobayashi, K.; Yogo, T.; Yamamura, S. Microstructure development and hydrogen gas interaction of oxidized $Zr_{65}Pd_{35}$ and $Zr_{60}Pd_{35}Ce_5$ amorphous alloys. *Jpn. J. Appl. Phys.* **2016**, *55*, 01AG05. [CrossRef]
33. Ozawa, M.; Katsuragawa, N.; Hattori, M.; Yogo, T.; Yamamura, S. Hydrogen absorption of Pd/ZrO_2 composites prepared from $Zr_{65}Pd_{35}$ and $Zr_{60}Pd_{35}Pt_5$ amorphous alloys. *Jpn. J. Appl. Phys.* **2018**, *57*, 01AF01. [CrossRef]
34. Panizon, E.; Ferrando, R. Solid-Solid Transitions in Pd-Pt Nanoalloys. *Phys. Rev. B* **2015**, *92*, 205417. [CrossRef]
35. Ishimoto, T.; Koyama, M. Electronic Structure and Phase Stability of PdPt Nanoparticles. *J. Phys. Chem. Lett.* **2016**, *7*, 736–740. [CrossRef]
36. Akamaru, S.; Hara, M.; Matsuyama, M. Alloying Effects on the Hydrogen-Storage Capability of Pd–TM–H (TM = Cu, Au, Pt, Ir) Systems. *J. Alloys Compd.* **2014**, *614*, 238–243. [CrossRef]
37. Kumara, L.S.R.; Sakata, O.; Kobayashi, H.; Song, C.; Kohara, S.; Ina, T.; Yoshimoto, T.; Yoshioka, S.; Matsumura, S.; Kitagawa, H. Hydrogen Storage and Stability Properties of Pd–Pt Solid-Solution Nanoparticles Revealed via Atomic and Electronic Structure. *Sci. Rep.* **2017**, *7*, 14606. [CrossRef] [PubMed]

38. Tayal, A.; Seo, O.; Kim, J.; Kumara, L.S.R.; Song, C.; Hiroi, S.; Chen, Y.; Kobayashi, H.; Kitagawa, H.; Sakata, O. Effects of Interfacial Structure of Pd–Pt Nanoparticles on Hydrogen Solubility. *J. Alloys Compd.* **2019**, *791*, 1263–1269. [CrossRef]
39. Tayal, A.; Seo, O.; Kim, J.; Kobayashi, H.; Yamamoto, T.; Matsumura, S.; Kitagawa, H.; Sakata, O. Mechanism of Hydrogen Storage and Structural Transformation in Bimetallic Pd–Pt Nanoparticles. *ACS Appl. Mater. Interfaces* **2021**, *13*, 23502–23512. [CrossRef]
40. Ozawa, M.; Matsubara, T.; Hattori, M. One-pot preparation of Pd–Pt alloy nanoparticles and their hydrogen gas interaction. *Jpn. J. Appl. Phys.* **2020**, *59*, SAAC04. [CrossRef]
41. El-Eskandarany, M.S.; Saida, J.; Inoue, A. Amorphization and crystallization behaviors of glassy Zr70Pd30 alloys prepared by different techniques. *Acta Mater.* **2002**, *50*, 2725–2736. [CrossRef]
42. Yamanaka, S.; Nishizaki, T.; Uno, M.; Katsura, M. Hydrogen Dissolution into Zirconium Oxide. *J. Alloys Compd.* **1999**, *293–295*, 38–41. [CrossRef]
43. Dubinin, M.M. Fundamentals of the theory of adsorption in micropores of carbon adsorbents: Characteristics of their adsorption properties and microporous structures. *Carbon* **1989**, *27*, 457–467. [CrossRef]
44. Nguyen, C.; Do, D.D. The Dubinin–Radushkevich equation and the underlying microscopic adsorption description. *Carbon* **2001**, *39*, 1327–1336. [CrossRef]
45. Hardy, B.; Corgnale, C.; Chahine, R.; Richard, M.-A.; Garrison, S.; Tamburello, D.; Cossement, D.; Anton, D. Modeling of adsorbent based hydrogen storage systems. *Int. J. Hydrogen Energy* **2012**, *37*, 5691–5705. [CrossRef]
46. Niemann, M.U.; Srinivasan, S.S.; Phani, A.R.; Kumar, A.; Goswami, D.Y.; Stefanakos, E.K. Nanomaterials for Hydrogen Storage Applications: A Review. *J. Nanomater.* **2008**, *2008*, 950967. [CrossRef]
47. Bardhan, R.; Hedges, L.O.; Pint, C.L.; Javey, A.; Whitelam, S.; Urban, J.J. Uncovering the intrinsic size dependence of hydriding phase transformations in nanocrystals. *Nat. Mater.* **2013**, *12*, 905–912. [CrossRef]
48. Griessen, R.; Strohfeldt, N.; Giessen, H. Thermodynamics of the hybrid interaction of hydrogen with palladium nanoparticles. *Nat. Mater.* **2016**, *15*, 11–17. [CrossRef]
49. Ozawa, M.; Todoroki, T.; Kato, H.; Hattori, M. The dependence of hydrogen storage properties on the sizes of Pd nanoparticles prepared by a solution-reduction method. *Jpn. J. Appl. Phys.* **2021**, *60*, SAAC05. [CrossRef]
50. Alekseeva, S.; Fanta, A.B.D.S.; Iandolo, B.; Antosiewicz, T.J.; Nugroho, F.A.A.; Wagner, J.B.; Burrows, A.; Zhdanov, V.P.; Langhammer, C. Grain boundary mediated hydriding phase transformations in individual polycrystalline metal nanoparticles. *Nat. Commun.* **2017**, *8*, 1084. [CrossRef]
51. Züttel, A. Materials for hydrogen storage. *Mater. Today* **2003**, *6*, 24–33. [CrossRef]
52. Rahm, J.M.; Löfgren, J.; Erhart, P. Quantitative predictions of thermodynamic hysteresis: Temperature-dependent character of the phase transition in Pd–H. *Acta Mater.* **2022**, *227*, 117697. [CrossRef]
53. Jin, Y.; Hara, M.; Wan, J.L.; Matsuyama, M.; Watanabe, K. Isotope Effects on Hydrogen Absorption by Pd–4at.%Pt Alloy. *J. Alloys Compd.* **2002**, *340*, 207–213. [CrossRef]
54. Akiba, H.; Kobayashi, H.; Kitagawa, H.; Ikeda, K.; Otomo, T.; Yamamoto, T.; Matsumura, S.; Yamamuro, O. Structural and Thermodynamic Studies of Hydrogen Absorption/Desorption Processes on PdPt Nanoparticles. *J. Phys. Chem. C* **2019**, *123*, 9471–9478. [CrossRef]